

#### **PAPER**

## 3D bioprinting using hollow multifunctional fiber impedimetric sensors

To cite this article: Alexander P Haring et al 2020 Biofabrication 12 035026

View the <u>article online</u> for updates and enhancements.



## **Biofabrication**



RECEIVED 2 March 2020

z iviaicii 202

REVISED 29 April 2020

ACCEPTED FOR PUBLICATION 20 May 2020

PUBLISHED
29 June 2020

#### **PAPER**

# 3D bioprinting using hollow multifunctional fiber impedimetric sensors

Alexander P Haring<sup>1,2,9</sup>, Shan Jiang<sup>3,9</sup>, Catherine Barron<sup>4</sup>, Emily G Thompson<sup>5</sup>, Harald Sontheimer<sup>5,6</sup>, Jia-Qiang He<sup>4</sup>, Xiaoting Jia<sup>3,7</sup> and Blake N Johnson<sup>1,2,6,7,8,10</sup>

- Department of Industrial and Systems Engineering, Virginia Tech, Blacksburg, VA 24061, United States of America
- Macromolecules Innovation Institute, Virginia Tech, Blacksburg, VA 24061, United States of America
- <sup>3</sup> Bradley Department of Electrical and Computer Engineering, Virginia Tech, Blacksburg, VA 24061, United States of America
- Department of Biomedical Sciences and Pathobiology, Virginia-Maryland College of Veterinary Medicine, Blacksburg, VA 24061, United States of America
- <sup>5</sup> Glial Biology in Health, Disease and Cancer Center, Carilion Fralin Biomedical Research Institute, Roanoke, VA 24016, United States of America
- <sup>6</sup> School of Neuroscience, Virginia Tech, Blacksburg, VA 24061, United States of America
- Department of Materials Science and Engineering, Virginia Tech, Blacksburg, VA 24061, United States of America
- Department of Chemical Engineering, Virginia Tech, Blacksburg, VA 24061, United States of America
- These authors contributed equally to this work.
- $^{10}\,$  Author to whom any correspondence should be addressed.

E-mail: bnj@vt.edu

**Keywords:** 3D bioprinting, sensors, impedimetric sensors, stem cell bioprinting, process monitoring Supplementary material for this article is available online

#### Abstract

3D bioprinting is an emerging biofabrication process for the production of adherent cell-based products, including engineered tissues and foods. While process innovations are rapidly occurring in the area of process monitoring, which can improve fundamental understanding of process-structure-property relations as well as product quality by closed-loop control techniques, in-line sensing of the bioink composition remains a challenge. Here, we report that hollow multifunctional fibers enable in-line impedimetric sensing of bioink composition and exhibit selectivity for real-time classification of cell type, viability, and state of differentiation during bioprinting. Continuous monitoring of the fiber impedance magnitude and phase angle response from 10<sup>2</sup> to 10<sup>6</sup> Hz during microextrusion 3D bioprinting enabled compositional and quality analysis of alginate bioinks that contained fibroblasts, neurons, or mouse embryonic stem cells (mESCs). Fiber impedimetric responses associated with the bioinks that contained differentiated mESCs were consistent with differentiation marker expression characterized by immunocytochemistry. 3D bioprinting through hollow multifunctional fiber impedimetric sensors enabled classification of stem cells as stable or randomly differentiated populations. This work reports an advance in monitoring 3D bioprinting processes in terms of in-line sensor-based bioink compositional analysis using fiber technology and provides a non-invasive sensing platform for achieving future quality-controlled bioprinted tissues and injectable stem-cell therapies.

#### 1. Introduction

The increasing demands for products capable of repairing injuries and treating diseases have driven the growth of the regenerative medicine industry [1–6]. While various biofabrication processes have been examined for tissue engineering, demands for product prototyping and personalization have driven the creation of computer-aided biofabrication processes, such as 3D bioprinting processes. 3D

bioprinting of cell-laden tissue constructs involves a number of pre-processing operations, including cell differentiation and expansion processes [7, 8], cell separation processes [8, 9], and bioink preparation steps. Thus, while there are various process parameters that are important toward the fabrication of repeatable bioprinted tissues, such as bioink rheological properties, there is a need for real-time in-line bioink compositional analysis, including concentration, cell type, and cell viability, for scalable and

quality-controlled fabrication of 3D bioprinted constructs.

3D bioprinting processes have various process parameters, each of which exhibit a unique measurement strategy and challenge. One particularly challenging aspect from a process monitoring approach is the use of animal cells, often human cells, as a processed material, which have been referred to as 'living materials' from a processing perspective. While sensors are emerging for compositional analysis in cell expansion bioreactors [10], there remains a need for sensing platforms capable of continuous in-line monitoring of bioink composition and cell quality measures, such as viability and state of differentiation, during bioprinting. For example, in addition to potential variability in cell expansion, differentiation outcome, and bioink preparation steps, processing defects such as nozzle clogging can also lead to inconsistency among 3D bioprinted tissue constructs.

Impedimetric-based sensing platforms has emerged as an attractive non-destructive testing approach for monitoring cell health, proliferation, and activity in both suspensions and adherent cultures [11]. For example, Nordberg et al demonstrated an impedance-based cell assay that monitored the impedance magnitude at 40 kHz in human adipose stem cell (hASC) cultures from young, middle aged, and elderly donors during proliferation and osteogenic differentiation [12]. In that study, sensor response enabled prediction of osteogenic potential in hASC populations, a result which has implications in quality-controlled biomanufacturing of stem cellbased therapies [12]. In another example, Sharma et al used impedance spectroscopy to investigate the viability of NS0 murine myeloma cells, an important cell line for production of therapeutic proteins, and found that impedance response enabled a more rapid detection of cell death than a Trypan blue staining assay as well as potential for continuous viability monitoring [13]. Narayanan et al used dielectric impedance spectroscopy for monitoring the quality of 3D bioprinted constructs [14]. This work showed that monitoring of permittivity change, Cole-Cole slope factor, and critical polarization frequency correlated with cell viability and proliferation and were significantly affected by printing parameters such as processing time and temperature [14]. Thus, an impedimetric sensing approach that could be integrated with the bioink deposition tool (e.g. nozzle) of the 3D bioprinting process may be particularly useful for in-line real-time bioink compositional and quality analysis throughout the material deposition process.

Multifunctional fibers with hollow channels have emerged as attractive platforms for chronic neural monitoring applications given their integrated sensing and microfluidic-based drug delivery capabilities [15, 16]. For example, Canales *et al* reported hollow polymer fibers which allowed simultaneous drug delivery, optical stimulation, and neural recording

for long-term experiments in transgenic Thy1-ChR2-YFP mice [17]. In this study, CNQX, an AMPA receptor antagonist, was injected through the fibers and electrophysiological measurements were made during optogenetic stimulation before and after the injection demonstrating successful injection, stimulation, and measurement [17]. In another study, Park et al injected viral vectors containing opsin genes into mouse brains, then optically stimulated the brain and monitored neural electrophysiological response [18]. This demonstrated ability to simultaneously inject a fluid and obtain electrical measurements makes microfluidic multifunctional fibers an attractive platform for impedimetric sensing of bioink composition and quality during continuous extrusion.

Here, we present a fiber-based impedimetric sensor for monitoring of bioink composition and quality during continuous microextrusion. Extrusion through electrode-functionalized hollow fibers enabled continuous monitoring of cell-laden solution or bioink impedance magnitude |Z| and phase angle  $(\phi)$  of the extrudate. Studies using fibroblasts, neuronal cells, and stem cells showed that impedimetric sensing enabled detection of cell type, state of differentiation, and viability. This report provides an advance in sensor-based monitoring of 3D bioprinting processes based on bioink compositional and quality analysis using hollow multifunctional fiber technology. Overall, hollow multifunctional fibers provide an attractive platform for controlled delivery and fabrication of cell therapies.

### 2. Experimental

#### 2.1. Materials

Alginic acid sodium salt from brown algae (alginate) and calcium chloride (CaCl<sub>2</sub>) were purchased from Sigma-Aldrich. Nanofibrillated cellulose (NFC) was purchased from the University of Maine Product Development Center. RPMI-1640 was from American Type Culture Collection (ATCC). Horse serum was from Gibco. Fetal bovine serum (FBS) was from Aleken Biologicals. Penicillin-streptomycin, Dulbecco's Modified Eagle Medium (DMEM)/F12 medium, DPBS, Trypsin EDTA, Hoechst 33 342, calcein AM, and ethidium homodimer-1 (EthD-1) were from Thermo Fisher. High-glucose DMEM was from GE Healthcare Life Sciences. ES-cell qualified FBS was from ZenBio (Research Triangle, NC). Leukemia inhibitory factor (LIF; 1000 U ml<sup>-1</sup>) was from Pepro-Tech (Rocky, NJ). Nonessential amino acids (NEAA) was from Quality Biological Inc. (Gaithersburg, MD). 2-mercaptoethanol (2-ME) was from Sigma-Aldrich (St. Louis, MO). L-glutamine was from Quality Biological Inc. Penicillin-streptomycin (1X) was from (VWR) Radnor, PA. Polycarbonate (PC) film was from Laminated Plastics. Medical epoxy (EA M-121HP) was from Henkel Loctite. Silver paint was from SPI Supplies. Vinyl acetate tubing (0.5 mm

inner diameter) and polyvinylidene fluoride was from McMaster-Carr. 5-minute epoxy was from Devcon.

#### 2.2. Hydrogel preparation

Alginate solutions were prepared by dissolving alginate in DPBS at room temperature under constant stirring for 24 h. An alginate concentration of 1 wt% was prepared for fibroblast and neuronal cell experiments, and a concentration of 0.25 wt% was prepared for mouse embryonic stem cell experiments. Following preparation, 2 wt% NFC was added to the 1 wt% alginate solution used for fibroblast and neuronal cell 3D printing and homogenized under sonication for 90 s (FB705 with microtip accessory, Fisher Scientific). All solutions were autoclaved at 121 °C for 30 min prior to use.

#### 2.3. Cell culture and differentiation

Neuronal cells from the rat adrenal gland (PC-12, ATCC) were cultured in RPMI-1640 supplemented with 10% v/v horse serum, 5% v/v FBS, and 100 U ml<sup>-1</sup> penicillin-100  $\mu$ g ml<sup>-1</sup> streptomycin at 37 °C and 5% CO<sub>2</sub>. The PC-12 cells grew as a suspension. The cell medium was changed twice weekly. PC-12 cells for low-viability bioinks were prepared via nutrient deprivation for one week, which was initiated when the culture reached confluence.

Mouse embryonic fibroblasts (NIH/3T3, ATCC) were cultured in DMEM/F12 supplemented with  $100 \text{ U ml}^{-1}$  penicillin- $100 \mu \text{g ml}^{-1}$  streptomycin and 10% v/v FBS at  $37 \,^{\circ}\text{C}$  and  $5\% \text{ CO}_2$ . The 3T3 cells grew as adherent cultures. Passaging was performed using treatment with Trypsin-EDTA solution at 90% confluency.

The mouse embryonic stem cells (mESCs) (C57BL/6; Cat. SCRC-1002; ATCC) were cultured in 0.1% gelatin-coated plates at 37 °C, 21%O<sub>2</sub> and 5%CO<sub>2</sub> with high-glucose DMEM supplemented with 15% ES-cell qualified FBS, 1000 U ml<sup>-1</sup> leukemia inhibitory factor, 0.1 mM nonessential amino acids, 0.1 mM 2-mercaptoethanol, 2 mM L-glutamine, and 1X penicillin streptomycin with daily medium change. To induce spontaneous differentiation, mESCs were washed twice with phosphate-buffered saline (PBS) and then cultured in the same medium, except in the absence of LIF. Medium was changed daily.

## 2.4. Fabrication of hollow multifunctional fibers

Similar to previous functional fibers [17], PC films were first wrapped around a Teflon rod (diameter = 6.35–12.7 mm) and placed in a heated oven (T = 200 °C). After the consolidation of the materials by heating, the Teflon rod was removed, resulting in a uniform PC tube. Single grooves (diameter = 3.175–4.37 mm) were then machined on opposite sides of the tube surface. A thin layer of PVDF (thickness = 0.12 mm) and thick layer of PC (thickness = 3 mm) were then rolled on the machined

PC tube. The assembly was then placed in a vacuum oven to facilitate material forming and consolidation. A copper wire (16 gauge) was passed through each of the two channels that remained from the machining process to complete the fabrication of the preform. Hollow multifunctional fibers were subsequently drawn from the preform using a thermal drawing process, which was performed under controlled temperature and stress using a custom furnace (temperatures in the pre-heating section, heating section, and cooling section were 150, 285, and 110 °C, respectively). Fiber drawing was done at constant velocity (85 cm min<sup>-1</sup>).

Upon initial production of the fiber, the copper electrodes were exposed on both ends of the fiber. To prevent contact between the electrodes and the extrudate at both the entrance and exit to the fiber, the exposed electrodes at the entrance were blocked with medical epoxy. This ensured the two electrodes would only contact the material at one location, at the exit of the fiber. To provide an opening for connecting leads to the copper wires embedded in the fiber, a scalpel was used to remove material along a section of the outer walls of the fiber exposing the embedded copper wire. Silver paint was used to connect the exposed copper wire in the fiber to copper leads. To build the fluidic connection, the fiber was inserted into the ethylene vinyl acetate tubing (0.5 mm inner diameter) and the whole device was affixed with 5min epoxy. The tubing was slid onto 18-gauge syringe tips to form a tight se

#### 2.5. 3D bioprinting of cell-laden bioinks

Following cell resuspension in fresh pre-warmed growth medium, cell-laden bioinks were then created by combining cell suspensions and 2 wt% alginate solutions at a 1:1 ratio by volume. 2 ml of 1 wt% cell-laden alginate bioinks with 2 wt% NFC were loaded into sterile 5 cc syringe barrels with 500  $\mu$ m diameter tips that contained the hollow fibers. Tips and fibers were sterilized with 70% ethanol prior to use. The PC-12 and 3T3 cells were collected as a single-cell suspension in phosphate-buffered saline (PBS, Fisher) following dissociation with Trypsin-EDTA (3T3) or Accutase (PC-12, Sigma). The cell concentration and percent of viable cells was determined using Trypan Blue (VWR) following manufacturer's instructions. Based on the Trypan blue counts, bioinks containing  $5 \times 10^5$  and  $1 \times 10^6$  PC-12 cells ml<sup>-1</sup>, 1  $\times$  10<sup>6</sup> 3T3 fibroblasts ml<sup>-1</sup>, and  $5 \times 10^5$  dead PC-12 cells ml<sup>-1</sup> were prepared. All tissue constructs were printed into 6-well plates using a commercial 3D bioprinter (Inkredible+, CELLINK) using extrusion pressures ranging from 2 to 10 psi at a print speed of 1 mm s<sup>-1</sup>. Following printing, 500  $\mu$ l of sterile 100 mM CaCl<sub>2</sub> was applied to each sample and allowed to cure for 120 s before triple rinsing with 2 ml sterile DPBS. All bioprinting was done in a biosafety cabinet. All studies were done using single-layer square tissue constructs  $(10 \times 10 \text{ mm}^2)$ . Single-layer constructs were selected to prevent tissue necrosis during culture associated with diffusion-limited transport, which is an established challenge to biofabrication of macroscopic tissues and motivation for the creation of vascularized tissues. Each experimental group contained (n=6) replicates.

#### 2.6. Syringe extrusion of cell-laden bioinks

2 ml of 0.25 wt% cell-laden alginate bioinks containing  $10^6$  cells ml $^{-1}$  were prepared and loaded into 5 ml syringes. Suspensions containing stable stem cells (+LIF) and spontaneously differentiated cells (-LIF) were prepared at the same concentration. Sterile tips that contained the hollow fibers (diameter =  $500 \, \mu \text{m}$ ) were then attached to the syringe. Cell-laden bioinks were hand printed based on a previously reported technique [19] into petri dishes and subsequently cured with  $500 \, \mu \text{l}$  of sterile  $50 \, \text{mM}$  CaCl $_2$  by exposure for  $120 \, \text{s}$  followed by triple rinsing with 2 ml sterile DI water.

#### 2.7. Sensing principle and data acquisition

The configuration of the hollow multifunctional fiber sensor is based on impedance analysis of the circuit composed of the two fiber copper electrodes and the extruded material, which is in the middle of the copper electrodes. The electrical impedance response of the system was done using a potentiostat (Interface 1010E, Gamry Instruments) using a two-electrode format in which one copper electrode served as the working electrode, the other copper electrode served as the counter electrode using an AC voltage of 10 mV and zero DC offset over a range of 0.100–100 kHz in a logarithmic sweep with 10 points per decade.

### 2.8. Immunocytochemistry

The mESC and differentiated mESC cells were fixed with 4% paraformaldehyde (PFA) at room temperature for 30 min and then cytospun onto glass tissue slides at 1100 revolutions per minute (RPM) for 4 min. The resulting cells were then washed twice with PBS, followed by blocking in 1.5% BSA and 0.2% Tween20 buffer for 1 h at room temperature. The cells were then incubated overnight with 1:250 anti-stage specific embryonic antigen-1 (SSEA-1, Santa Cruz Biotech, Dallas, TX), washed thrice, and stained with a secondary antibody, goat anti-mouse 594, at a concentration of 1:1000 in blocking buffer. Hoechst 33 342 was counterstained to label cell nuclei in all groups. An additional set of coverslips were stained with only secondary antibody as a negative control. Fluorescent micrographs were acquired using an Olympus IX73 microscope equipped with a DP70 CCD camera (Olympus, Center Valley, PA). The images were then analyzed using ImageJ software (NIH). At least 1100 Hoechst cells were analyzed in

each group to calculate percent of SSEA-1-positive cells over total number of cells.

#### 2.9. Live/dead assay of PC-12 and 3T3 cells

At days 1 and 7 following printing, cell viability was assessed with a LIVE/DEAD Assay (Thermo Fisher) following manufacturer's instructions. In brief, the bio-printed parts were incubated in a 2  $\mu$ M calcein AM and 4  $\mu$ M EthD-1 solution for 30 min at 37 °C with 5% CO<sub>2</sub>. The bio-printed parts were then moved into fresh cell medium for imaging using a laserscanning microscope (A1R; Nikon) equipped with a Plan Apo 10×/N.A 0.45 air objective. Two independent fields of view were imaged per sample for each condition. Quantification of the percentage of cells that were viable was performed with ImageJ Fiji software. In short, the total volume of cells (green signal from calcein AM and red signal from EthD-1) was calculated by creating a binary representation of the fluorescent signals. Subsequently, the percentage of viable cells was obtained by dividing the calcein AM (green signal) volume from the calculated total volume.

# 2.10. Live/dead assay of mESCs and spontaneously differentiated cells

Cured alginate hydrogels were dissolved with the addition of 0.1 M EDTA. Bioprinted mESC and differentiated mESC cells were centrifuged at 1100 RPM for 4 min and then suspended in 1 ml culture medium to remove alginate. Cells were then plated in a 0.1% gelatin-coated 48-well plate (1  $\times$  10 $^5$  cells per well) and allowed 2 h to attach to the bottom of the culture dish. Afterward, cells were washed with PBS and incubated with 2  $\mu$ M calcein AM, 1.25  $\mu$ M EthD-1, and 1  $\mu$ M Hoechst 33 342 for 20 min. Cells were imaged with Olympus IX73 microscope described above and analyzed using ImageJ software. At least 800 Hoechst cells were analyzed in each group to calculate percentage of dead cells over total number of cells.

The calcein AM/EthD-1 staining was also performed for cells 72 h following 3D bioprinting, except the cells were cultured and imaged in the hydrogel. The percentage of dead cells was calculated by dividing total red (representing dead cells) fluorescent intensity over total blue (representing total number of cells) fluorescent intensity for each image.

#### 2.11. Statistics

Statistical analysis was completed in Origin Pro 2016. Student's t-test were used for live/dead and SSEA-1 assays. Chi-squared tests were used for Trypan blue counts. \*, \*\*, and \*\*\* indicate a p-value (p) less than 0.05, 0.01, and 0.001, respectively. Error bars and  $\pm$  indicate standard deviation. Number of replicates (n) is specified for each experiment and was greater than three in all cases.

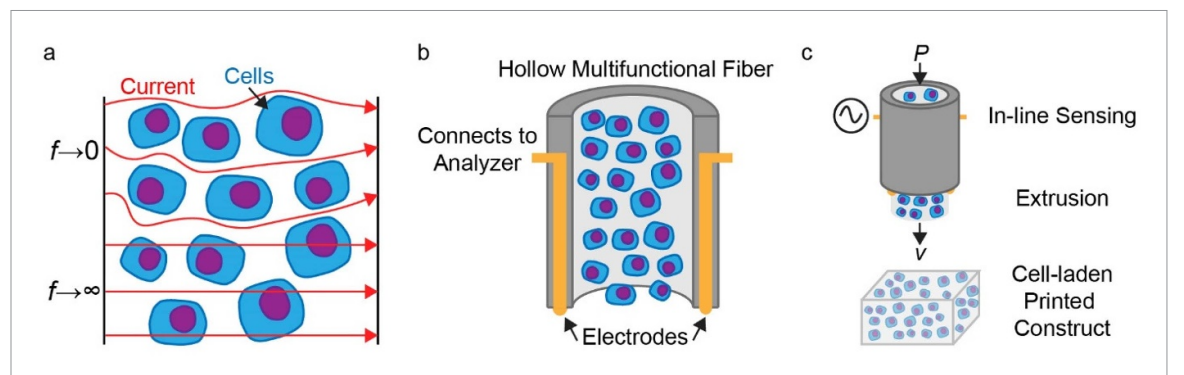


**Figure 1.** (a) Schematic representation of impedimetric monitoring of cell-laden materials using a two-electrode format showing the paths of current when driven by low-  $(f \to 0)$  and high-frequency  $(f \to \infty)$  applied potentials. (b) Schematic showing the impedimetric sensing principle for bioink compositional analysis implemented in hollow multifunctional fibers. (c) Schematic describing the concept of sensor-based in-line bioink compositional analysis of 3D bioprinting processes using multifunctional fibers.

#### 3. Results and discussion

# 3.1. Principle of in-line bioink compositional analysis for 3D bioprinting processes using hollow multifunctional sensors

Impedimetric sensing is a useful characterization technique for enabling in-line monitoring of cellladen bioink composition and quality, given it can be acquired non-invasively via boundary electrodes and can be performed with high-sampling rates. As shown in figure 1(a), the flow of alternating current through cell-laden materials, such as tissues, is dependent on the frequency of the applied electrical potential [20]. At low frequency, the current is dominated by charge transfer around cells through the extracellular matrix (ECM) or extracellular fluid (ECF), while current also arises from charge transfer through cells at high frequency [20]. To date, impedimetric characterization of cell-laden materials has enabled the characterization of cell shape, size, density, and integrity [11, 20]. As shown in figure 1(b), hollow multifunctional fibers enable impedimetric characterization of extruded materials, such as a cell-laden bioink, using the two copper fiber electrodes. Thus, multifunctional fibers potentially enable real-time monitoring of the bioink impedance magnitude (|Z|) and phase angle ( $\phi$ ) frequency response during extrusion. As shown in figure 1(c), hollow multifunctional fibers facilitate in-line sensing of 3D bioprinting processes, particularly realtime bioink compositional analysis. A schematic of the sensor design and nozzle integration approach is shown in figure 2(a). Photographs showing the sensor following the fabrication process and integration with the nozzle are provided in figures 2(b) and (c), respectively. As shown in figures 2(a) and (c), the sensor was anastomized to the nozzle by inserting the nozzle into the sensor tubing component. Importantly, the sensor design provides a non-invasive, inline process monitoring format that avoids the need for extensive modification of the bioprinting process. Multifunctional fibers potentially provide an attractive sensing platform for understanding the

effect of bioink composition and process parameters, such as extrusion flow rate, on the properties and quality measures of 3D bioprinted tissue constructs.

# 3.2. Fabrication of hollow multifunctional fibers for extrusion of cell-laden bioinks

Given the majority of microextrusion 3D bioprinting is done using extrusion nozzles of diameters ranging from 100-500  $\mu$ m [21-23], we first examined the ability to tune the fiber channel diameter by varying the fiber design or thermal drawing process parameters. As shown in figure 3(a), we produced the electrode-functionalized hollow fibers of conserved cross-sectional geometry and composition using the thermal drawing process. Before the thermal drawing process, we first created a macroscopic template, a preform, by wrapping PC films around a mandrel (Teflon rod), consolidating them, and machining the structure. The final preform consisted of one center hollow channel and two side hollow channels. Two copper wires were inserted into the two side channels respectively and they were confined within their initial grooves and remained adjacent to the center hollow channel using a convergence fiber drawing method as previously reported [24]. We varied the diameter of the center hollow channel by utilizing Teflon rods with different sizes. For example, the diameters of the Teflon rod used in this study were 6.35, 9.525, and 12.7 mm, which produced the corresponding hollow channel diameters in as-drawn fibers of 181, 272, and 362  $\mu$ m, respectively. In addition to modifying the fiber channel diameter through the dimensions of the Teflon rod used in the preform fabrication process, we further tuned the channel diameter by adjusting the draw down ratio defined as the ratio of initial to final diameter. Fibers with a range of commonly used inner diameters of 100, 200, 300, 400, and 500  $\mu$ m were fabricated by adjusting the draw down ratio used for the three aforementioned preform geometries (see figures 3(b)–(d) for representative micrographs of the fiber cross section;

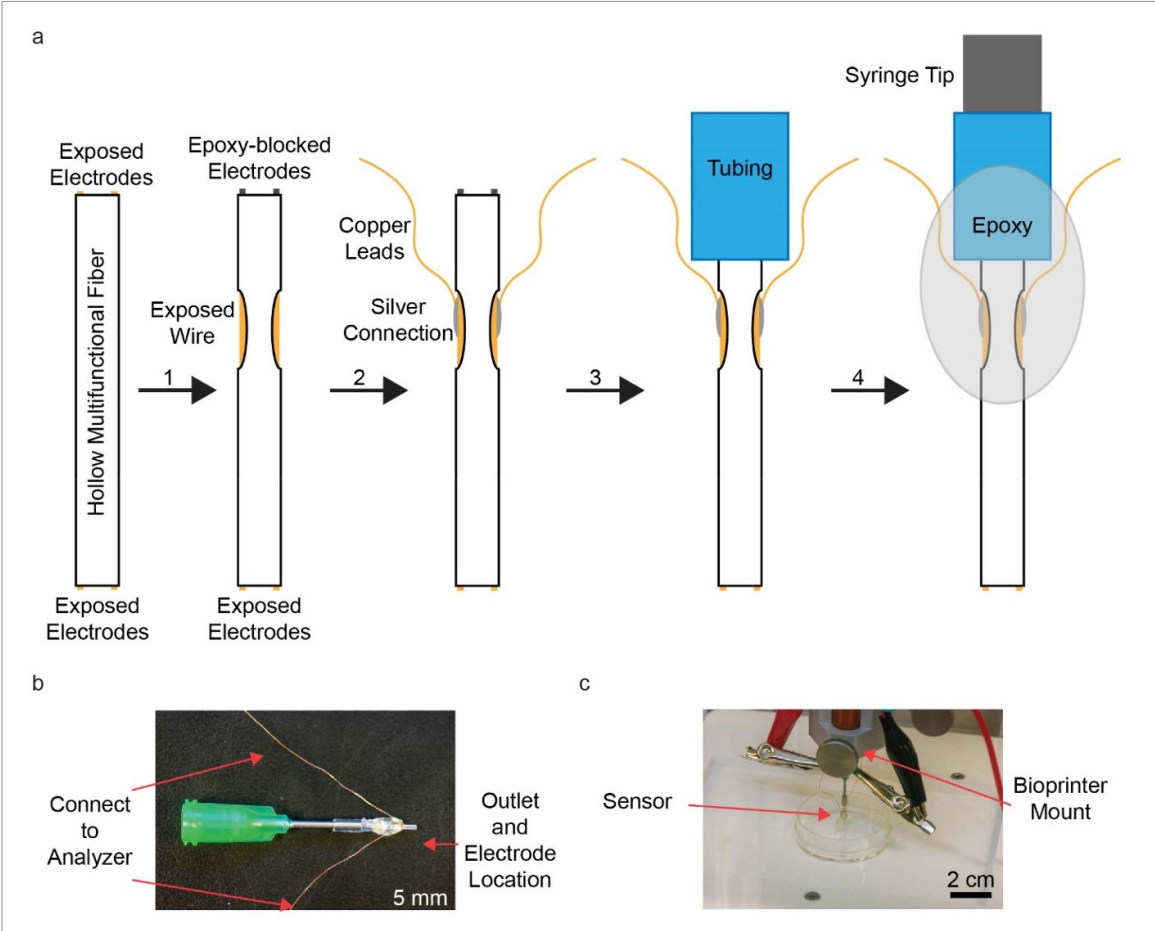


Figure 2. (a) Schematic illustrating the wire bonding process that enables interface between the electroded multifunctional fiber and the potentiostat. Step 1: Electrodes at the distal end of the fiber near the 3D bioprinting nozzle were blocked with medical epoxy. Cladding material was subsequently removed from the outer walls of the fibers to expose the embedded copper wire. Step 2: Copper leads were subsequently bonded to the exposed copper wires using a silver epoxy. Step 3: The fiber was then inserted into tubing. Step 4: 5-minute epoxy was then used to seal and reinforce the tubing-fiber connection and the bonded copper leads. The bioprinting nozzle was subsequently inserted into the tubing forming a tight seal that prevented the backflow of bioink. (b) Photograph of nozzle-fiber sensor assembly. (c) Photograph illustrating 3D bioprinting through the hollow multifunctional fiber impedimetric sensor.

micrographs of all fabricated fiber diameters can be found in supplementary figure S1 (available online at stacks.iop.org/BF/12/035026/mmedia)). Thus, the thermal drawing process enables the fabrication of hollow multifunctional fibers with a range of channel dimensions that are commonly employed for 3D bioprinting processes. As shown in figure 3(e), the volumetric flow rate (*Q*) increased nonlinearly with respect to increasing fiber channel diameter at a constant pressure, an expected result considering the Hagen-Poiseuille equation for shear-thinning power-law fluid (e.g. alginate solutions [25]) [26]:

$$Q = \frac{\pi R^3}{\frac{1}{n} + 3} \left(\frac{\Delta PR}{2LK}\right)^{1/n} \tag{1}$$

where n is the flow behavior index, K is the flow consistency index, R is the nozzle radius,  $\Delta P$  is the pressure drop, and L is the length of the nozzle [27]. The frictional head loss  $(h_f)$ , an important parameter relating to shear stress-induced cell death and injury in 3D bioprinting processes, was calculated using

Bernoulli's equation assuming negligible contributions of potential energy effects as [26]:

$$h_f = \frac{P_{appl} - P_{atm}}{\rho g} - \frac{v_{out}^2}{2g} \tag{2}$$

where  $P_{appl}$  is the applied pressure (here, 5 psi),  $P_{atm}$  is atmospheric pressure,  $v_{out}$  is the average velocity at the outlet, g is the acceleration due to gravity, and  $\rho$  is the density of the fluid. We note that equation (2) ignores the effect of head loss due to contraction effects, which is a valid assumption in laminar flow regimes [26]. The head loss per unit length ( $S = h_f IL$ ) can be related to the Darcy friction factor ( $f_D$ ) through the Darcy-Weisbach equation as [28]:

$$f_D = \frac{\pi^2 g D^5 S}{8Q^2}$$
 (3)

The mean wall shear stress ( $\tau$ ) that cells are exposed to during the 3D bioprinting process can subsequently be estimated in terms of the Darcy-Weisbach friction factor as [29]:

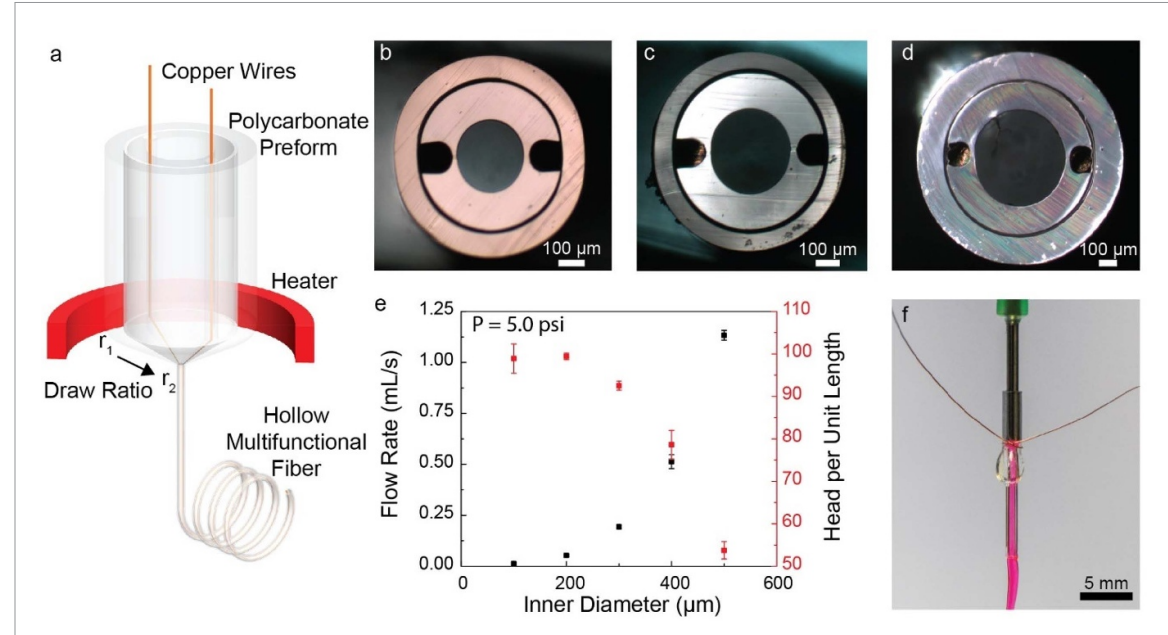


**Figure 3.** (a) Schematic of the manufacturing process to produce electrode functionalized hollow multifunctional fibers. A preform tube with imbedded copper wires was drawn, and the draw down ratio controlled the fiber diameter. Cross sections of drawn fibers with inner diameters of 300 (b), 400 (c), 500  $\mu$ m (d). (e) Volumetric flow rate of water in ml s<sup>-1</sup> and head per unit length through 34.0 mm long fibers from an applied pressure of 5.0 psi. (f) Image of gel extrusion through a 500  $\mu$ m diameter fiber, red dye added for visibility.

$$f_D = \frac{\pi^2 g D^5 S}{8Q^2} \tag{4}$$

As shown in figure 3(e), the head loss per length ranged from 98.9  $\pm$  3.4 to 53.7  $\pm$  2.0 over the diameter range 100 to 500  $\mu$ m. While this study provides insight into the roughness of the fiber channel walls and illustrates the ability to understand 3D bioprinting quality in terms of quantitative estimates of the shear stress experienced by cells, it should be noted that the shear stress generated in practice can be reduced by decreasing the average outlet velocity of the printed bioink (i.e. the speed of the 3D bioprinting process) as shown in equation 4. As shown in figure 3(f), hollow multifunctional fibers enabled continuous extrusion of alginate bioinks with minimal die swell at the average outlet velocities (i.e. extruder feed rates) for the 3D bioprinting studies discussed in the following sections.

# 3.3. Detection of cell viability differences among extruded cell-laden bioinks via fiber-based impedimetric monitoring

Understanding the effects of material (i.e. bioink) properties and process parameters, such as bioink rheological properties and average velocity of extruded bioink, respectively, on resultant tissue quality remains an active area of research within the biofabrication field. For example, material innovations, such as those based on novel shear-thinning bioinks, are continuing to emerge that reduce the shear stress-induced cell damage and death during 3D bioprinting. Given that the viability of deposited cells is among the most important characteristics

to quantify and monitor from a process and quality control perspective, we next examined if the hollow multifunctional fibers could detect the viability of cells within extruded cell-laden bioinks. As shown in figures 4(a) and (b), alginate-NFC bioinks containing PC-12 cells with either high or low viability at the same concentration of  $5 \times 10^5$  cells ml<sup>-1</sup> exhibited different impedance responses over the frequency range of 0.1 to 100 kHz and different phase angle responses over the range of 0.1 to 2 kHz. Live/dead stained images taken following bioprinting can be seen in figure 4(c). Each micrograph in figure 4(c)depicts both live (green) and dead (red) cells to highlight the qualitative difference in viability between the healthy and dead experimental bioink groups. The difference in viability is quantified in figure 4(d), the bioinks containing populations of cells with either high or low viability exhibited 89.8  $\pm$  2.8% and 0% viability. As shown in figure 4(a), bioinks that contained a high population of viable cells exhibited a higher impedance than those that contained a high population of dead cells across the 0.1 to 100 kHz frequency range. The difference was significant from 10-20 kHz (p < 0.05). The maximum relative difference in impedance between the two bioinks of 118% was observed at 12 kHz. This result agrees with previous impedimetric results, and is attributed to the integrity of the cell membranes [30, 31]. As shown in figure 4(b), bioinks that contained a high population of viable cells exhibited a relatively higher phase angle in the low frequency range. Differences in phase angle between the two bioinks were not distinguishable above 2 kHz. The difference in phase angle between the bioinks was significant from

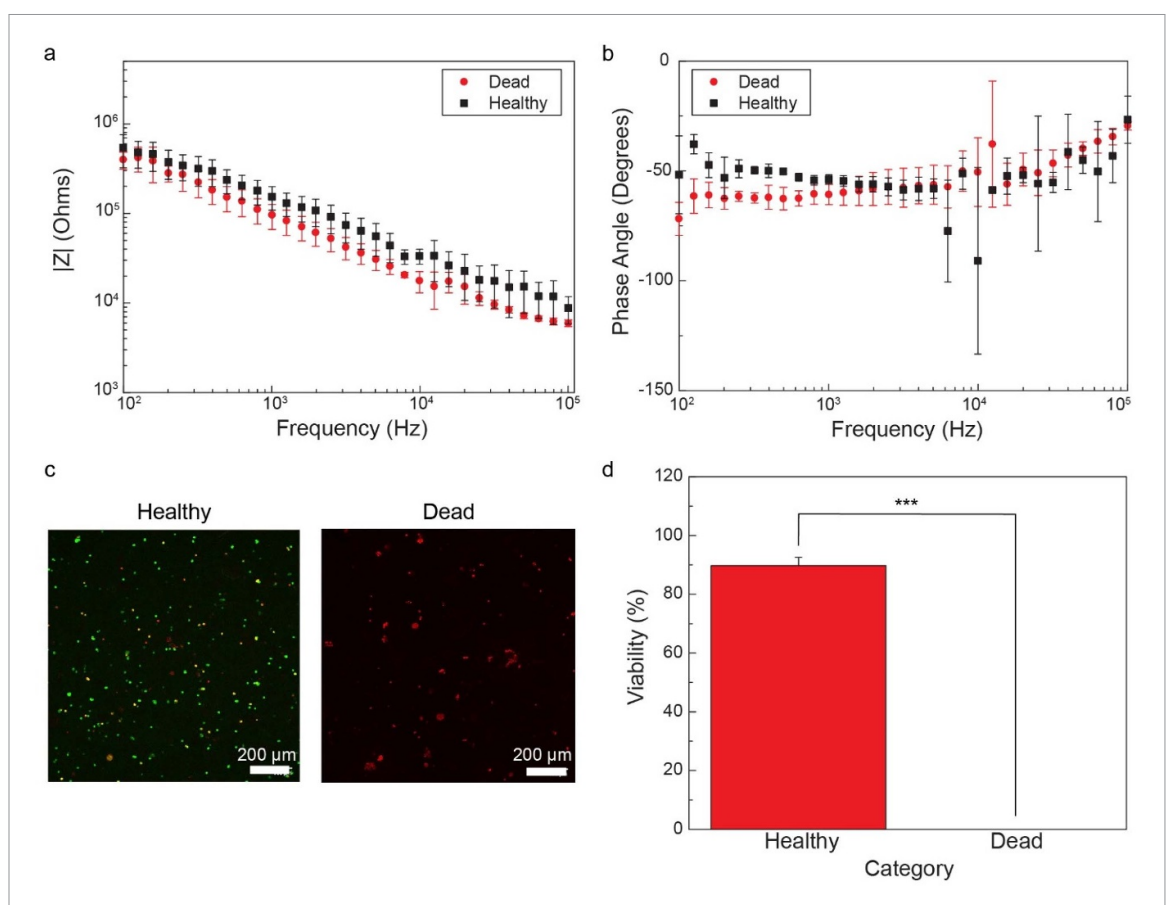


**Figure 4.** Electrical impedance spectra of hollow multifunctional fibers during 3D bioprinting of cell-laden alginate-NFC bioinks containing  $5 \times 10^5$  cells ml $^{-1}$  shown in terms of the impedance magnitude (a) and phase angle (b) responses (error bars correspond to the standard deviation of measurements obtained from bioprinting of n=3 constructs). (c) Fluorescence micrographs associated with a live/dead stain of bioinks containing populations of PC-12 cells with either high or low viability. (d) Viability study of bioinks containing populations of PC-12 cells with either high or low viability (n=3 biological replicates, \*\*\* indicates p < 0.001).

0.1-0.6 kHz (p < 0.05). The maximum difference in phase angle between the two bioinks of 13.6° was observed at 0.16 kHz. Thus, fixed-frequency impedance and phase angle monitoring of extruded cellladen bioinks at frequencies ranging from 10-20 kHz (e.g. 12 kHz) and 0.1-0.6 kHz, respectively, could potentially enable real-time monitoring of cell viability in 3D-printed bioinks at high sampling rates (i.e. temporal resolution). Bioprinted constructs fabricated using the viable bioink were cultured for seven days. We found that the cell viability in the bioprinted tissue constructs was 76.5  $\pm$  8.1% after the curing process (day 1) and did not significantly differ from the cell viability on day 7 (81  $\pm$  2.8%) (see supplementary figure S2 for associated live/dead stains).

# 3.4. Detection of cell type differences among extruded cell-laden bioinks via fiber-based impedimetric monitoring

Having shown that 3D bioprinting using hollow multifunctional fibers enables detection of cell viability differences among cell-laden bioinks, we next examined whether they could also characterize differences in cell type. While many bioprinted constructs

are composed of a single cell type, applications of 3D bioprinting to fabrication of organ-on-a-chip system requires bioprinting of multiple cell types on a single substrate [32–34]. In addition to the fabrication of organ-chip platforms, applications of 3D bioprinting to the design of chemotactic signals [35] and production of cell-laden scaffolds for repair of complex injuries [34] often requires deposition of multiple cell types in a single construct. As shown in figures 5(a) and (b), alginate-NFC bioinks containing either PC-12 cells or fibroblasts at the same concentration of  $1 \times 10^6$  cells ml<sup>-1</sup> exhibited different impedance responses over the frequency range of 0.1 to 100 kHz. Live/dead stained images taken following bioprinting can be seen in figure 5(c). As shown in figure 5(d), the PC-12 cell- and 3T3 cell-laden bioinks exhibited cell viabilities of 70.5  $\pm$  5.8 and 92.5  $\pm$  4.2%, respectively. As shown in figure 5(a), bioinks that contained PC-12 cells exhibited a higher impedance than those containing 3T3 cells across the 0.1 to 100 kHz frequency range. The difference was significant from 0.1-2 kHz (p < 0.05). The maximum relative difference in impedance between the two bioinks of 153% occurred at 0.1 kHz, which was different than the location of the maximum impedance

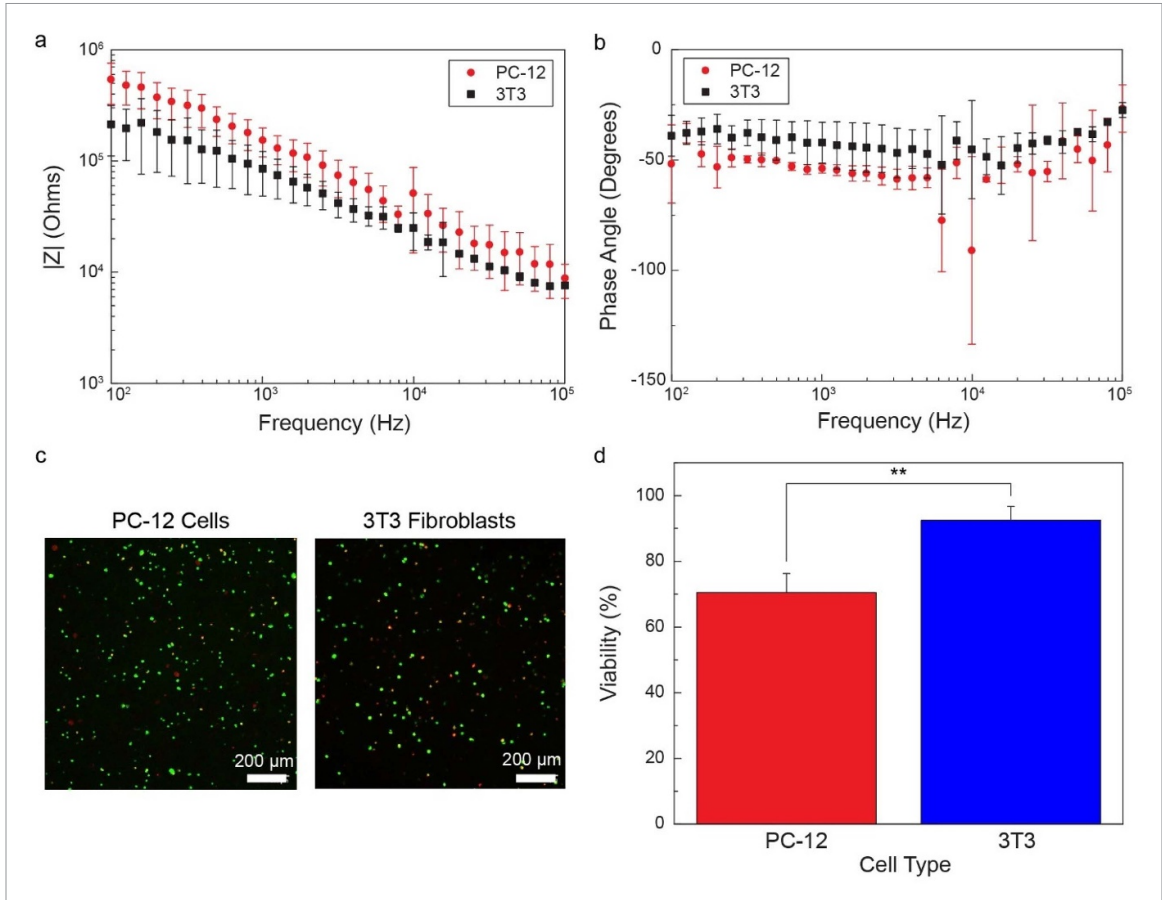


**Figure 5.** Electrical impedance spectra of hollow multifunctional fibers during 3D bioprinting of PC-12 cell- and 3T3 cell-laden alginate-NFC bioinks containing  $1 \times 10^6$  cells ml<sup>-1</sup> shown in terms of the impedance magnitude (a) and phase angle (b) responses (error bars correspond to the standard deviation of measurements obtained from bioprinting of n = 3 constructs). (c) Fluorescence micrographs associated with a live/dead stain of bioinks containing viable PC-12 or 3T3 cells. (d) Viability study of PC-12 or 3T3 cell-laden bioinks (n = 3 biological replicates, \*\* indicates p < 0.01).

difference associated with sensing of bioink cell viability (12 kHz) (see figure 5(a)). While the data in figure 4(a) suggest that one might expect the PC-12 cell-laden bioinks to exhibit a lower impedance than those that contain 3T3 cells based on their relative viabilities, the data in figure 5(a) suggest that other differences among the cell types, such as size and morphology, dominate viability effects in terms of the impedance response. As shown in figure 5(b), bioinks that contained PC-12 cells exhibited a lower phase angle than those that contained 3T3 cells across the 0.1 to 100 kHz frequency range, however, the differences were not significant at a 95% confidence interval. Thus, fixed-frequency impedance monitoring of extruded bioinks at 0.1-2 kHz could potentially enable real-time monitoring of cell type in 3D-printed bioinks at high sampling rates. Bioprinted constructs fabricated using the viable bioink were cultured for seven days. The 3D bioprinted PC-12 cell- and 3T3 cell-laden bioprinted tissue constructs exhibited day-7 cell viabilities of 74.6  $\pm$  7.4 and 87.0  $\pm$  2.1%, respectively (see supplementary figure S3 for associated live/dead stains).

# 3.5. Signal response to stem cells and differentiated cells

In addition to the ability to detect changes in cell viability and types, the ability to classify the state of 3D bioprinted cells remains an important process monitoring challenge, particularly for biofabrication of quality 3D bioprinted stem cell therapies. Given stem cell pluripotency and stability are required for effective function of associated 3D bioprinted stem cell therapies, it remains a present biomanufacturing challenge to preserve pluripotency and maintain stem cell stability during processing based on the tendency of stem cells to spontaneously differentiate into terminal cell types [36]. Having shown that 3D bioprinting using hollow multifunctional fibers enables detection of cell viability and cell type differences among cell-laden bioinks, we next examined if they could also characterize differences in the extent of differentiation among stem cells comprising a stem cellladen bioink. Embryonic stem cells can be stabilized in a self-renewing state through the application of leukemia inhibitory factor (LIF) [37, 38]. As shown in figures 6(a) and (b), alginate bioinks containing mESCs at  $1 \times 10^6$  cells ml<sup>-1</sup> cultured in the presence

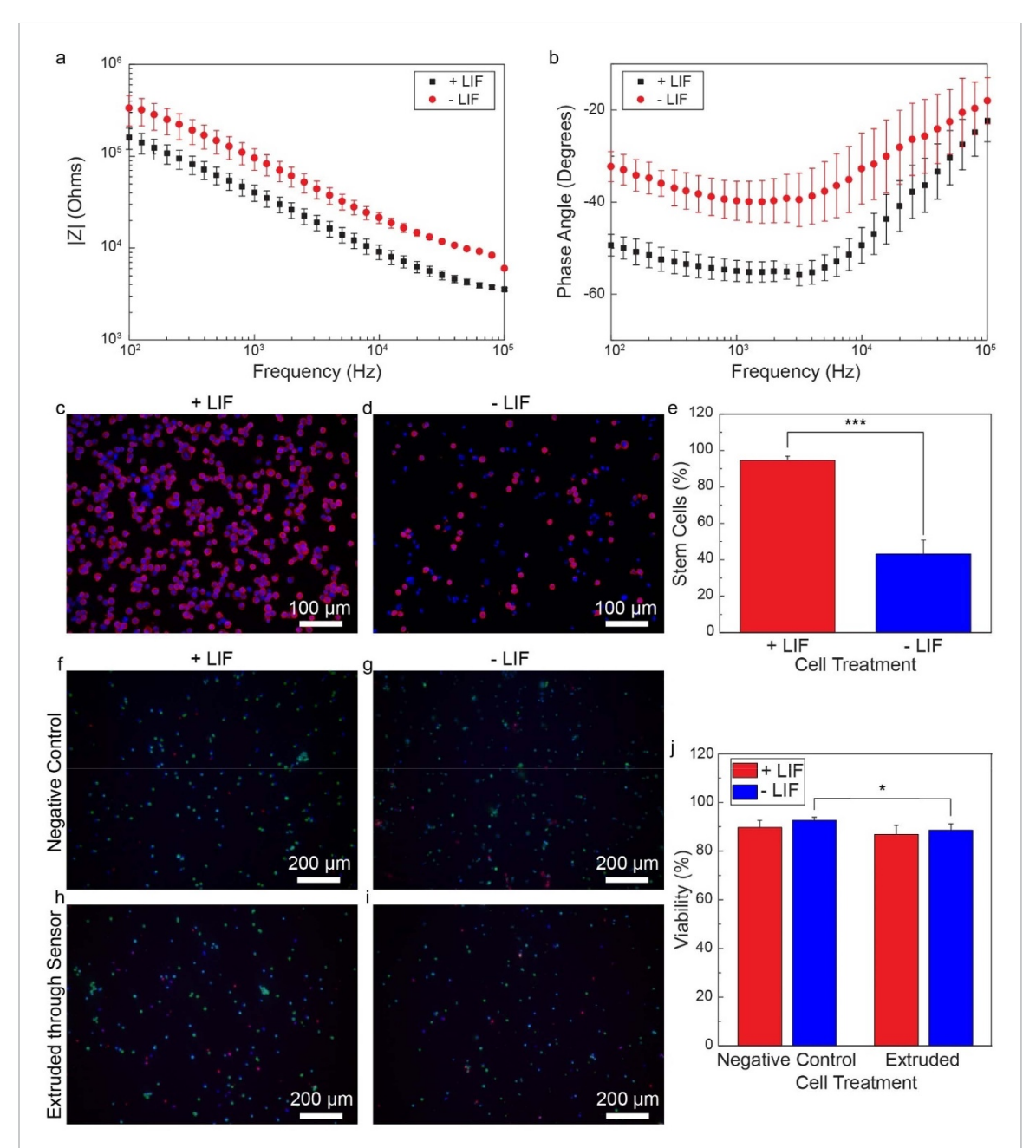


**Figure 6.** Impedance magnitude (a) and phase angle (b) of stem cells (+LIF) and spontaneously differentiated cells (-LIF), averages of n=3 samples shown. Merged fluorescent micrographs (200x) associated with expression of SSEA-1, a mESC specific marker, in mESC cultures stabilized in a stem cell state (+LIF) (c) and allowed to spontaneously differentiate (-LIF) (d), which served the basis of the stem cell-laden bioinks. (e) Percentage of stem cells present in a stem cell state based on SSEA-1 expression data following 14 d of culture in +LIF and -LIF media (i.e. panels c and d) (\*\*\* indicates p < 0.001, n=3). Fluorescent micrographs (100x) associated with live/dead assays of stem cells in a stem cell state (+LIF) (f) and (g) and in a spontaneously differentiated state (-LIF) (h) and (i) in both bioprinted and molded constructs using calcein AM, EthD-1, and Hoechst 33 342 (nuclei). (j) Summary of stem cell viability following processing (\* indicates p < 0.05, n=3).

or absence of LIF exhibited distinguishable impedance responses across the 0.1–100 kHz frequency range. As shown in figures 6(a) and (b), bioinks that contained a high population of stem cells (94.1% stem cells; +LIF) exhibited a lower impedance and phase angle than those in which a significant fraction of stem cells (56.8% differentiated cells; -LIF) had undergone differentiation across the 0.1 to 100 kHz frequency range. As shown in figure 6(a), the difference in impedance between the two bioinks ranged

from 69% at 100 kHz to 136% at 1 kHz, but the differentiated group (-LIF) exhibited a higher impedance across the 0.1 to 100 kHz frequency range (p < 0.05). The highest signal to noise level was achieved above 30 kHz. As shown in figure 6(b), the largest difference in phase angle between the bioinks occurred in the 0.1–5 kHz frequency range, with the maximum difference of 17.1° occurring at 0.1 kHz. The differences in phase angle were significant from 0.1–40 kHz (p < 0.05).

As shown in figures 6(c) and (d), mouse embryonic stem cells (mESCs) exhibited significant differences in expression of stage specific embryonic antigen-1 (SSEA-1), an established stemness marker, after culture in the presence or absence of LIF for 14 d (+LIF and -LIF, respectively). As summarized in figure 6(e), stem cells cultured in the presence and absence of LIF (i.e. +LIF and -LIF, respectively) tested 94.1  $\pm$  2.1% and 43.2  $\pm$  7.6% positive for SSEA-1, respectively. As shown in videos S1 and S2 of supporting information, mESCs cultured in the absence of LIF entered mesodermal differentiation towards cardiac differentiation. The presence of these contractile cells (see videos S1 and S2) provides further evidence that the cells cultured in the absence of LIF are no longer stem cells.

To investigate the impact of extrusion through the hollow multifunctional fiber on stem cell viability, the viability of stem cells in 3D bioprinted constructs was compared with that in molded constructs, which served as the control group. Micrographs associated with the live/dead assay in the 3D bioprinted and molded stem cell-laden tissue constructs are shown in figures 6(f)–(i). As shown in figure 6(j), the extruded +LIF and -LIF stem cell-laden 3D bioprinted constructs exhibited similar viability (86.8  $\pm$  3.7% and 88.6  $\pm$  2.7%, respectively) and extrusion of stem cellladen bioinks through the hollow multifunctional fiber had a minimal effect on cell viability relative to the molding process (86.8  $\pm$  3.7% vs. 89.7  $\pm$  2.9% for the +LIF group, respectively, and 88.6  $\pm$  2.7% vs. 92.6  $\pm$  1.2% for the -LIF groups, respectively). As shown in supplementary figure S4, the stem cell-laden tissue constructs exhibited no significant differences in cell viability by day 3. While the slope of the impedance and phase angle spectra can also potentially facilitate classification and quantification of bioink attributes, as suggested by the high-frequency data in figure 6(b), the differences in spectra slope were not significant at a 95% confidence interval. These results suggest that hollow multifunctional fibers provide an attractive form factor for in-line monitoring of stemness and extent of differentiation in stem cellladen bioinks during extrusion and assembly using 3D bioprinting processes.

### 4. Conclusions

While various attributes of bioink quality exist, characterization and real-time monitoring of such attributes differ with respect to measurement approach and constraint. Here, we examined if fiber-based impedimetric sensing can facilitate monitoring of bioink compositional and quality attributes that cannot otherwise be characterized without destructive analysis of the bioink, as such attributes provide significant barriers to real-time in-line monitoring, and thus, opportunities for 3D bioprinting process monitoring, control, and quality assurance. Here, we demonstrate

the capability of in-line monitoring of cell-laden bioink composition and quality during 3D bioprinting processes via impedimetric sensing. 3D bioprinting using hollow electrode functionalized fibers with controlled inner diameter enabled impedance spectroscopy of cell-laden bioinks during extrusion across the 10<sup>2</sup> to 10<sup>6</sup> Hz frequency range. Monitoring of fiber electrical impedance was shown to enable sensing of bioink compositional characteristics, such as cell viability, type, and extent of stem cell differentiation. Statistical analyses revealed candidate frequencies for fixed-frequency impedance and phase angle tracking, as used for real-time monitoring of microelectromechanical systems, which provide high sampling rates (i.e. temporal resolution). This work shows that impedimetric monitoring of bioink extrusion processes using hollow multifunctional fiber sensors provides a potential path to sensor-based monitoring, control, and quality assurance of 3D bioprinting processes, particularly regarding in-line monitoring of deposited cell viability, type, stemness, and extent of differentiation. This work also suggests that fiber-based sensors may provide useful platforms for controlled delivery of cell therapies, such as injectable stem cell therapies.

### Acknowledgments

APH acknowledges support by the Virginia Tech Interdisciplinary Graduate Research Program for Regenerative Medicine. XJ acknowledges the support of the US National Science Foundation (ECCS-1847436). BNJ is grateful for the generous support of the US National Science Foundation (CMMI-1739318).

## **Conflict of interest**

The authors declare no conflicts of interest.

#### **ORCID iD**

Blake N Johnson https://orcid.org/0000-0003-4668-2011

#### References

- [1] Bártolo P, Chua C, Almeida H, Chou S and Lim A 2009 Biomanufacturing for tissue engineering: present and future trends *Virtual Phys. Prototyping* 4 203
- [2] Bajaj P, Schweller R M, Khademhosseini A, West J L and Bashir R 2014 3D biofabrication strategies for tissue engineering and regenerative medicine *Annu. Rev. Biomed. Eng.* 16 247
- [3] Murphy S V and Atala A 2014 3D bioprinting of tissues and organs Nat. Biotechnol. 32 773
- [4] Mironov V, Kasyanov V and Markwald R R 2011 Organ printing: from bioprinter to organ biofabrication line Curr. Opin. Biotechnol. 22 667
- [5] Mironov V, Visconti R P, Kasyanov V, Forgacs G, Drake C J and Markwald R R 2009 Organ printing: tissue spheroids as building blocks *Biomaterials* 30 2164

- [6] Pigeau G M, Csaszar E and Dulgar-Tulloch A 2018 Commercial scale manufacturing of allogeneic cell therapy Frontiers Med. 5 233
- [7] Kumar A and Starly B 2015 Large scale industrialized cell expansion: producing the critical raw material for biofabrication processes *Biofabrication* 7 044103
- [8] Aijaz A, Li M, Smith D, Khong D, LeBlon C, Fenton O S, Olabisi R M, Libutti S, Tischfield J and Maus M V 2018 Biomanufacturing for clinically advanced cell therapies *Nat. Biomed. Eng.* 2 362
- [9] Clomburg J M, Crumbley A M and Gonzalez R 2017 Industrial biomanufacturing: the future of chemical production *Science* 355 aag0804
- [10] Holzberg T R, Watson V, Brown S, Andar A, Ge X, Kostov Y, Tolosa L and Rao G 2018 Sensors for biomanufacturing process development: facilitating the shift from batch to continuous manufacturing Curr. Opin. Chem. Eng 22 115
- [11] Gamal W, Wu H, Underwood I, Jia J, Smith S and Bagnaninchi P 2018 Impedance-based cellular assays for regenerative medicine *Phil. Trans. R. Soc.* B 373 20170226
- [12] Nordberg R C, Zhang J, Griffith E H, Frank M W, Starly B and Loboa E G 2017 Electrical cell-substrate impedance spectroscopy can monitor age-grouped human adipose stem cell variability during osteogenic differentiation *Stem Cells Transl. Med.* 6 502
- [13] Sharma R, Blackburn T, Hu W, Wiltberger K and Velev O D 2014 On-chip microelectrode impedance analysis of mammalian cell viability during biomanufacturing *Biomicrofluidics* 8 054108
- [14] Narayanan L K, Thompson T L, Shirwaiker R A and Starly B 2018 Label free process monitoring of 3D bioprinted engineered constructs via dielectric impedance spectroscopy *Biofabrication* 10 035012
- [15] Chen R, Canales A and Anikeeva P 2017 Neural recording and modulation technologies Nat. Rev. Mater. 2 1
- [16] Frank J A, Antonini M-J and Anikeeva P 2019 Next-generation interfaces for studying neural function *Nat. Biotechnol.* 37 1013
- [17] Canales A et al 2015 Multifunctional fibers for simultaneous optical, electrical and chemical interrogation of neural circuits in vivo Nat. Biotechnol. 33 277
- [18] Park S et al 2017 One-step optogenetics with multifunctional flexible polymer fibers Nat. Neurosci. 20 612
- [19] Lozano R, Stevens L, Thompson B C, Gilmore K J, Gorkin Iii R, Stewart E M, In Het Panhuis M, Romero-Ortega M and Wallace G G 2015 3D printing of layered brain-like structures using peptide modified gellan gum substrates Biomaterials 67 264
- [20] Amini M, Hisdal J and Kalvøy H 2018 Applications of bioimpedance measurement techniques in tissue engineering J. Electr. Bioimpedance 9 142
- [21] Blaeser A, Duarte Campos D F, Puster U, Richtering W, Stevens M M and Fischer H 2016 Controlling shear stress in 3D bioprinting is a key factor to balance printing resolution and stem cell integrity Adv. Healthcare Mater. 5 326

- [22] Haring A P, Sontheimer H and Johnson B N 2017 Microphysiological human brain and neural systems-on-a-chip: potential alternatives to small animal models and emerging platforms for drug discovery and personalized medicine Stem Cell Rev. Rep. 13 381
- [23] Kang H-W, Lee S J, Ko I K, Kengla C, Yoo J J and Atala A 2016 A 3D bioprinting system to produce human-scale tissue constructs with structural integrity Nat. Biotechnol. 34 312
- [24] Yu L, Parker S, Xuan H, Zhang Y, Jiang S, Tousi M, Manteghi M, Wang A and Jia X 2020 Flexible multi-material fibers for distributed pressure and temperature sensing Adv. Funct. Mater. 30 1908915
- [25] Rezende R A, Bártolo P J, Mendes A and Filho R M 2009 Rheological behavior of alginate solutions for biomanufacturing J. Appl. Polym. Sci. 113 3866
- [26] McCabe W L, Smith J C and Harriott P 2017 *Unit Operations of Chemical Engineering* vol 7 (New York: McGraw-hill)
- [27] Bird R B 2002 Transport phenomena. Appl. Mech. Rev. 55 R1
- [28] Elger D F, Roberson J A, Williams B C and Crowe C T 2016 Engineering Fluid Mechanics (NJ: Wiley Hoboken)
- [29] Chaudhry M H 2005 Applied hydraulic transients (Berlin: Springer)
- [30] Palego C, Merla C, Ning Y, Multari C R, Cheng X, Molinero D G, Ding G, Luo X and Hwang J C M 2013 Broadband microchamber for electrical detection of live and dead biological cells 2013 IEEE MTT-S Int. Microwave Symp. Digest (MTT) 2–7 June 2013
- [31] Shafiee H, Sano M B, Henslee E A, Caldwell J L and Davalos R V 2010 Selective isolation of live/dead cells using contactless dielectrophoresis (cDEP) Lab. Chip. 10 438
- [32] Johnson B N, Lancaster K Z, Hogue I B, Meng F, Kong Y L, Enquist L W and McAlpine M C 2016 3D printed nervous system on a chip Lab. Chip. 16 1393
- [33] Xu T, Zhao W, Zhu J-M, Albanna M Z, Yoo J J and Atala A 2013 Complex heterogeneous tissue constructs containing multiple cell types prepared by inkjet printing technology *Biomaterials* 34 130
- [34] Merceron T K, Burt M, Seol Y-J, Kang H-W, Lee S J, Yoo J J and Atala A 2015 A 3D bioprinted complex structure for engineering the muscle–tendon unit *Biofabrication* 7 035003
- [35] Haring A P, Thompson E G, Hernandez R D, Laheri S, Harrigan M E, Lear T, Sontheimer H and Johnson B N 2020 3D Printed multiplexed competitive migration assays with spatially programmable release sources Adv. Biosyst. 4 1900225
- [36] Amit M and Itskovitz-Eldor J 2002 Derivation and spontaneous differentiation of human embryonic stem cells J. Anat. 200 225
- [37] Hall J, Guo G, Wray J, Eyres I, Nichols J, Grotewold L, Morfopoulou S, Humphreys P, Mansfield W and Walker R 2009 Oct4 and LIF/Stat3 additively induce Krüppel factors to sustain embryonic stem cell self-renewal Cell Stem Cell 5 597
- [38] Murray P and Edgar D 2001 The regulation of embryonic stem cell differentiation by leukaemia inhibitory factor (LIF) Differentiation 68 227